Process development of Continuous Fiber Additive Manufacturing with in-line impregnated thermoplastic composites

W. Van De Steene, K. Ragaert, J. Martens, L. Cardon
Ghent University, Department of Materials, Textiles and Chemical Engineering, Centre for Polymer and Materials Technologies, Ghent, Belgium

ABSTRACT: In previous research, three methods for the melt impregnation of continuous fiber bundles with a thermoplastic polymer were assessed. These impregnated composite strands would be an interesting material to use in an extrusion based Additive Manufacturing (AM) process. In applications where high stiffness and strength are required, this Continuous Fiber Additive Manufacturing (CFAM) technique could produce strong, stiff and lightweight composite parts as an alternative to metal products. This preliminary research focusses on the process development for printing both single and dual layer composites. Both single layer samples with a fiber volume fraction of around 40 vol%, with a decent fiber distribution in the matrix and also dual layer samples were successfully printed and characterized.

1 INTRODUCTION

Fused Filament Fabrication (FFF) has known a mayor increase in importance in Additive Manufacturing (AM) technologies during the last three decades. However, optimizations of this manufacturing process were often limited to machine and software developments.

Last years, there is a strong demand for additively manufactured parts that can be mechanically loaded, rather than being visual prototypes or casting patterns. Since, the development of new materials for FFF has been increasing. A first method to increase mechanical properties such as stiffness and strength is to use short glass, carbon of natural fibers as a filler material in a thermoplastic polymer, as seen in the work by Tekinalp et al. 2014, Ning et al. 2016, Compton et al. 2017, Ferreira et al. 2017, Raney et al. 2017, Kishore et al. 2017, Brenken et al. 2018 and Zhang et al. 2018. A disadvantage of the use of these composites is their increased brittleness (Fu et al. 2000, Compton et al. 2014) compared to the virgin polymer materials.

Another approach to increase stiffness and strength of thermoplastic materials, often by multiple orders of magnitude, is the use of continuous fiber reinforcement such as glass, carbon, aramid or natural fibers. This approach however requires an important adaptation of the FFF process. Two important production techniques are currently being researched. A first method intends to remelt a composite strand, existing of a fiber bundle, pre-impregnated in a powder coating oven (Nunes et al. 2003) or commingled with a thermoplastic polymer, in a heated nozzle right before deposition (Gardner et al. 2016, Melenka et al. 2016, Dickson et al. 2017, Eichenhofer et al. 2017, Goh et al. 2018). A second method combines both the impregnation and the deposition process in a single production step, as being researched by Bettini et al. 2016, Matsuzaki et al. 2016, Nanya et al. 2016, Tian et al. 2016, Van De Steene et al. 2016, Liu et al. 2018 and Van De Steene et al. 2018. The fiber fractions of the composites created in these researches is ranging from less than 1 vol% up to around 50 vol%, with strongly varying void content and fiber distribution and dispersion.

The main goal of this research is to prove that i) the “ActivePin” melt impregnation process that was proposed in previous research (Van De Steene et al. 2016, Van De Steene et al. 2018) is well-suited to be used in an additive manufacturing process, ii) that a fiber volume fraction of around 40 vol% can be achieved, iii) that a single layer can be printed with limited to no voids, iiii) that a second layer can be deposited on top of a first layer and iiiii) that fiber dispersion and distribution in the matrix material is similar to a uniform, theoretical distribution model.

2 MATERIALS AND METHODS

2.1 *Materials*

A polyamide 12 from Arkema, Rilsamid AMN O TLD, was used as the matrix material for the composites produced. Its density was determined according

to ISO 1183 to be 1092 ± 9 kg/m³ (confidence level 95%).

StarRov LFTplus Direct Roving 853 continuous glass fiber bundle from Johns Manville was used as the reinforcement material in the composite. The linear density was determined according to ISO 1889:2009 as 1179.29 ± 5,48 tex (confidence level 95%), which is equivalent to 2225 single fibers per bundle. Mean single fiber diameter was determined on a perpendicular polished cross section of an embedded fiber bundle as 16.29 ± 1.75 µm. Density of the fiber material is 2540 kg/m³.

2.2 *Continuous Fiber Additive Manufacturing (CFAM) process*

In Van De Steene et al. (2017), three methods (Pultrusion, PassivePin and ActivePin) for melt-impregnation of continuous fiber bundles with a thermoplastic polymer were proposed and evaluated. These impregnation methods can be performed in-line with an additive deposition technique. Therefore, the impregnation device (Figure 1) containing a polymer melt chamber (a) and impregnation pins (b) should be equipped with a puller mechanism (c) and a heated deposition nozzle (d) in order to perform an automated lay-up of thermoplastic composite material on the heated build platform (e) of an AM platform, often referred to as '3D-printer'. It is important for the deposition nozzle to have a rounded transition to gently guide and smear out the wetted fiber bundle without the occurrence of fiber failure. For an isotropic fiber material with single fiber diameter **d**, Young's modulus **E** and bending strength $\boldsymbol{\sigma_b}$, the minimum bending radius **R** can be estimated according to Equation 1:

$$R \geq \frac{E\,d}{\sigma_b} \qquad (1)$$

This condition should be taken into account for all applied bends on the fiber bundle throughout the whole impregnation and deposition process to prevent fiber failure and clogging of the pultrusion or deposition system.

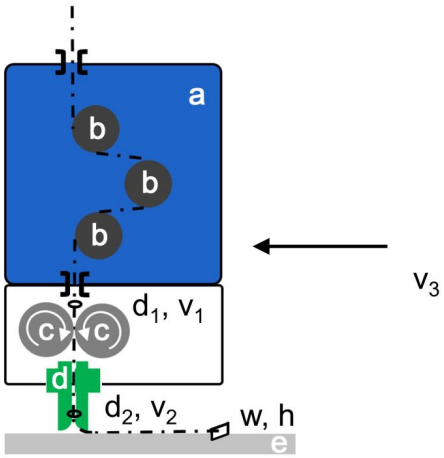

Figure 1: pultrusion device with deposition system.

2.3 *Development of an AM platform for CFAM*

A custom AM platform that is able to handle the composite lay-up forces was developed. It is a cartesian system with a build platform moving in X-, Y- and Z-axis and a stationary deposition system. This configuration allows the use of heavy composite or pellet based extruders.

The build environment is fully enclosed and thermally insulated. The build platform can be operated at temperatures up to 180°C to avoid uneven shrinkage, internal stresses and delaminations. Also, interdiffusion between different deposited strands can be improved by deposition at a higher build chamber temperature due to a higher annealing effect, as described by Spoerk et al. (2018).

2.4 *CFAM extrusion kinematics*

In a typical Fused Deposition Modeling Additive Manufacturing process, or in its open-source counterpart Fused Filament Fabrication, a round filament with diameter $\mathbf{d_1}$ is fed through a heated nozzle with an internal diameter $\mathbf{d_2}$, which is often a factor 5 to 7 smaller than $\mathbf{d_1}$. This implies that the filament feeding speed is typically a factor 25 to 50 smaller than the relative movement of the printhead to the build platform. This difference in velocity is possible due to the very limited melt strength of the thermoplastic polymers used in the process.

In CFAM however, the velocity $\mathbf{v_1}$ (Figure 1) at which the continuous fiber composite is pulled through the melt chamber and through a pultrusion die with diameter $\mathbf{d_1}$ should be equal to the velocity of the composite in the nozzle $\mathbf{v_2}$ and equal to the deposition velocity $\mathbf{v_3}$ (Equation 2). This requires that the composite's cross section area will be constant throughout the lay-up process, however, it can change shape. To obtain a fully dense composite part, theoretically the composite strand's circular cross section should be smeared out to a rectangular one, having a layer height **h**, a strand width **w** and correction factor **c** which takes into account the imperfection of the rectangular cross section and a polymer leakage flow between the fiber bundle and the pultrusion die **(**Equation 3). Due to processing considerations, the diameter of the nozzle $\mathbf{d_2}$ can be chosen slightly larger than the pultrusion die diameter (Equation 4).

$$v_1 = v_2 = v_3 \qquad (2)$$

$$d_1 = c\,w\,h \qquad (3)$$

$$d_2 \geq d_1 \qquad (4)$$

During preliminary testing, the composite strand extrusion velocity $\mathbf{v_1}$ and deposition velocity $\mathbf{v_3}$ were matched during the iterative printing of a straight line. In the case that $\mathbf{v_1} < \mathbf{v_3}$ the deposited strand was pulled loose from the polyetherimide build platform. In the opposite case, being $\mathbf{v_1} > \mathbf{v_3}$, the unwanted effect of buckling of the strand was noticed, either within the nozzle (causing obstructions) or after deposition (causing an instable composite deposition).

2.5 *Single and dual layer CFAM tests*

In FFF, the occurrence of sharp corners in the tool paths is trivial. In order to deposit a single layer of continuous fiber composite onto the build platform, an extra difficulty should be considered. Due to the high stiffness of the composite material, minimum bending radii should be applied in the tool path to avoid both high stresses in the fibers and 'tow buckling' and 'tow pullup' (Lukaszewicz et al. 2012). Thereto, a custom software code for creating tool paths was written where a minimum bending radius of 1.25 mm was applied at every directional change in the tool paths. In Figure 2, an example of such a tool path for a single layer specimen consisting of 6 parallel composite strands is shown, dimensions for a single layer are 100 x 16 x 0.6 mm. A dual layer sample was created by repeating this pattern on top of a first layer without staggering. All samples were produced using a pultrusion die with diameter 1.3 mm and a pultrusion speed of 1 mm/s. Temperature of the melt chamber and the deposition nozzle was set at 240°C, the build platform's temperature was chosen 110°C.

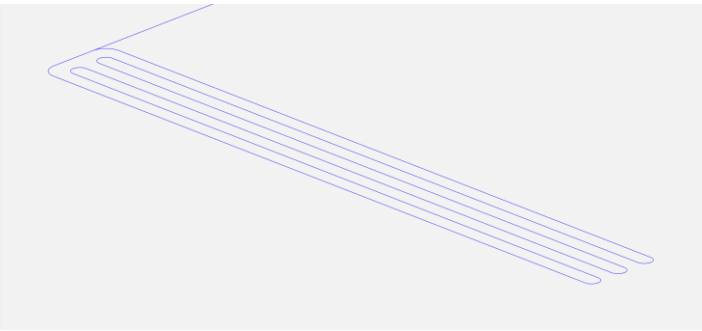

Figure 2: tool path for a single layer composite specimen, 100 x 16 x 0.6 mm.

2.6 *Optical microscopy on composite cross sections*

Both single and dual layer composite samples were embedded in 'Epofix', a cold curing epoxy from Struers. The embedded samples were cut perpendicular to the fiber direction and polished up to a 4000 grit silicon carbide.

Micrographs were made on a Keyence VHX-2000 digital microscope at a magnification of 250. This magnification allows for studying fiber distribution and dispersion, processing-morphology effects and void formation in the composite.

2.7 *Fiber volume fraction determination*

To get an idea about obtainable mechanical properties for a composite processing technique and thus its possible field of applications, the rules of mixture can be used: knowing the mechanical properties of the composite's constituents, the fiber volume fraction $\mathbf{V_f}$ and matrix volume fraction $\mathbf{V_m}$ or void volume fraction $\mathbf{V_v}$, mechanical properties of the composite can be estimated. Following relation between these volume fractions is valid (Equation 5):

$$V_f + V_m + V_v = 1 \quad (5)$$

The composites' $\mathbf{V_f}$ is determined mainly by the diameter of the pultrusion die $\mathbf{d_1}$. Also the pultrusion velocity might have an influence on $\mathbf{V_f}$ due to the shear-thinning effects of the polymer melt and thus the fiber-polymer ratio. Due to possible leakage of the polymer between the pultrusion die bore and the fiber bundle, a calculation of $\mathbf{V_f}$ based on $\mathbf{d_1}$ and the linear density of the fiber bundle is only an estimate (Van De Steene et al. 2017). A more accurate method for $\mathbf{V_f}$ determination is incineration of the deposited composite to determinate fiber mass fraction $\mathbf{M_f}$ (Equation 6) and matrix mass fraction $\mathbf{M_m}$, (Equation 7). In a single layer composite $\mathbf{V_v}$ can be neglected, meaning $\mathbf{V_f}$ can be derived from $\mathbf{M_m}$, the matrix's density $\boldsymbol{\rho_m}$ and the fiber's density $\boldsymbol{\rho_f}$ using Equation 8. In dual layer samples, which are prone to have larger interlayer voids, a correction for $\mathbf{V_v}$ should be made. This value can be derived from void area measurements on the made micrographs or from micro tomography void measurements.

$$M_f = \frac{m_f}{m_c} \quad (6)$$

$$M_m = \frac{m_c - m_f}{m_c} \quad (7)$$

$$V_f = \frac{V_m \rho_m (1 - M_m)}{\rho_f M_m} \quad (8)$$

Composite samples with dimensions 10 x 16 x 0.6 mm were cut out of a single layer composite plate, weighted on a Precisa XR 205SM-DR scale (composite sample mass $\mathbf{m_c}$) and incinerated in a Nabertherm LT 6/11/R7 oven for 15 minutes at a temperature of 550°C. Afterwards, the samples were weighted anew to determine the remaining fiber

mass $\mathbf{m_f}$ to be able to calculate the matrix mass $\mathbf{m_m}$ lost on incineration.

2.8 *Quantisation of fiber dispersion and distribution in a composite*

Consider a circular cross section perpendicular to the fiber direction of a unidirectional composite material. The cross section contains **n** unique fibers, each of which can be represented by the polar coordinates (radius $\mathbf{r_i}$ and polar angle $\boldsymbol{\phi_i}$) measured at its center.

By determining all pairwise distances $\mathbf{d_{ij}}$ between each fiber center using Equation 9, fiber distribution and dispersion can be characterized in a histogram. For an idealized fiber distribution in the circular cross section, a normal distribution is expected. All fiber distribution imperfections in an actual composite cross section will have their consequence on the shape of the cross section's Bell curve, which can be quantified in parameters such as mean, standard deviation, skewness and (excess) kurtosis values.

$$d_{ij} = \sqrt{r_i^2 + r_j^2 - 2r_i\, r_j \cos\left(\phi_i - \phi_j\right)} \qquad (9)$$

3 RESULTS AND DISCUSSION

3.1 *Optical microscopy results*

A micrograph of a single layer composite cross section was made (Figure 3a). Visually, it can be seen that the matrix material of the individual strands is interdiffused, however spots with a lower fiber content can be distinguished in the weld zones between the six deposited strands. Within a single strand, fibers seem to have a decent distribution, which will be characterized in paragraph 3.3. On the micrograph of a dual layer composite (Figure 3b), it can be noticed that the interdiffusion between adjacent strands of the second layer is limited due to some larger triangular voids. Also, between the first and the second layer, a moderate adhesion can be noticed, recognizable by the small (darker) voids. Both phenomena are related: due to its limited adhesion on the previous layer, a newly deposited strand is curling up, causing the triangular voids. In further research, these effects should be minimised by optimising layer thickness and nozzle and print environment temperature settings.

3.2 *Fiber volume fraction results*

The fiber volume fraction $\mathbf{V_f}$ of the single layer glass fiber – PA12 composite was determined to be 38,8 ± 1 % (confidence level 95%) in an incineration test. In this calculations, $\mathbf{V_v}$ was not taken into account due to the limited occurrence of voids (Figure 3a). It is concluded that a fiber volume fraction of 40 vol% is a realistic goal for the CFAM process. By changing the diameter of the pultrusion die, other fiber volume fractions can be achieved.

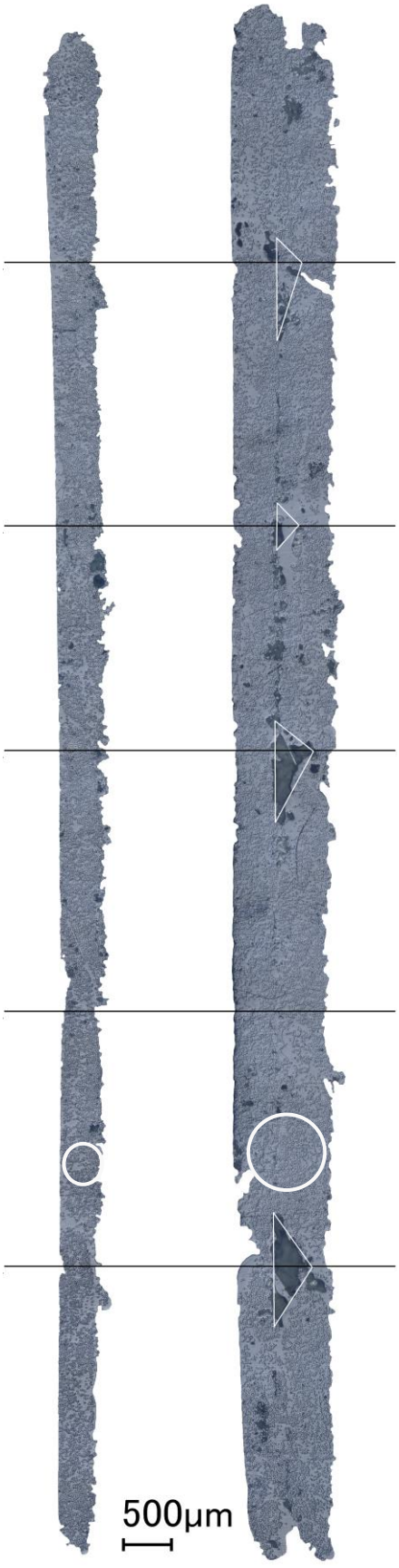

Figure 3: a) single layer cross section, weld zones shown as black lines (left), b) dual layer cross section (right), triangular voids marked in white. Both samples were produced with the left side of the cross section on the print bed.

3.3 *Quantisation of fiber dispersion and distribution results*

A circular section with a diameter of 0.5 mm in the micrograph in Figure 3a and a circular section with diameter 1 mm (including the interface between the two layers) in Figure 3b were considered for the quantisation of the fiber dispersion and distribution as described in paragraph 2.8. All pairwise distances $\mathbf{d_{ij}}$ were calculated and are shown in histograms in respectively Figure 4 and Figure 5. For both data sets, a decent fit with a normal distribution was found (Bell curves shown on graphs in narrow line). Statistical parameters such as mean inter-fiber distance and its standard deviation, skewness and kurtosis are given in Table 1 for both single layer and dual layer composites.

The standard deviation of the inter-fiber distances correlates with the fiber distribution in the matrix material: when the fibers are well distributed over the complete circular section, standard deviation will be maximal. The standard deviation values in Table 1 have a value of about 46% of their mean inter-fiber distance, indicating a decent fiber distribution.

The positive skewness, meaning that the mass of the distribution is concentrated left and the histogram has a right tail, shows that there is a light tendency of the fibers to coagulate, i.e. have a bad dispersion. Since negative inter-fiber distances are physically impossible, the right tail is larger than the left tail. The occurrence of fibers that are packed too close to each other can cause high local stresses in the matrix material and will play an important role in failure mechanisms. For this reason, a non-skewed distribution (skewness is zero) is preferred.

It can be noticed that the excess kurtosis is negative for both single and dual layer composites. Visually, it can be seen that mass of the distribution is concentrated more in intermediate values than in the mean value and outliers. This parameter describes the shape of the histogram and is for that reason an important parameter to fully characterize the composite material.

After comparing the single layer and dual layer composites, it is clear that both have very similar statistical parameters, showing that the morphology of both composites is very similar. Also, small differences could be a consequence of the different sample size (310 fibers in single layer dataset versus 1196 fibers in the dual layer dataset). This statistical technique for characterization could be an interesting way for quantifying fiber dispersion and distribution in a composite, especially when larger sample cross sections can be evaluated.

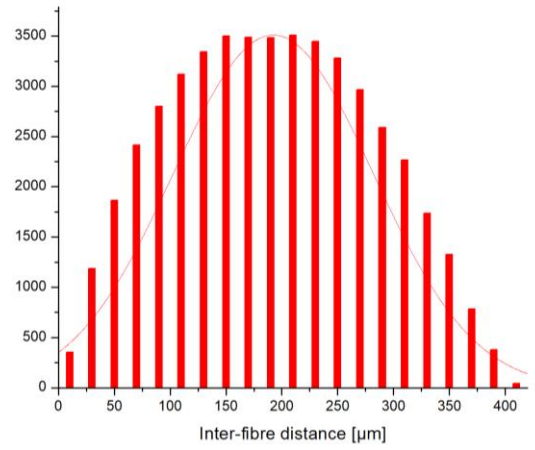

Figure 4: pairwise inter-fiber distances histogram on a 0.5 mm circular section of a single layer composite.

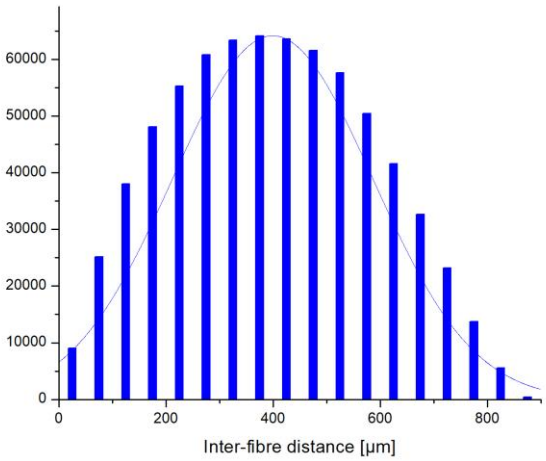

Figure 5: pairwise inter-fiber distances histogram on a 1 mm circular section of a dual layer composite.

Table 1: Bell curve parameters characterizing fiber distribution and dispersion of a single and a dual layer composite.

	Single layer	Dual layer
Mean distance	192	399
Standard deviation	89	187
Skewness	0.088	0.108
Excess kurtosis	-0.85	-0.80

4 CONCLUSIONS AND OUTLOOK

The aim of this research was to evaluate the feasibility of the use of the “ActivePin” melt impregnation technique in an AM process. In order to demonstrate this, both single and dual layer unidirectional continuous glass fiber – PA12 composites with dimensions 100 x 16 x 0.6 mm were successfully produced.

Incineration of the composites showed that a fiber fraction of 38,8 ± 1 vol% (confidence level 95%) was obtained.

Single layer composites showed a limited void content and a proper interdiffusion of the matrix material in the weld zones between the adjacent strands. Between the layers of the dual layer composite, only a moderate adhesion was established and triangular voids were found between adjacent strands in the second layer. In future work, parameters such as layer height and deposition nozzle temperature and print environment temperature could be optimized to enhance the composite's quality.

On the micrographs of the composites' perpendicular cross section, fiber distribution and dispersion were studied. Analysis of the pairwise distances between the fibers proved to be a relevant method to quantify the fibers' distribution and dispersion. Parameters such as mean inter-fiber distance, standard deviation, skewness and kurtosis were used to model the pairwise inter-fiber distance's statistical distribution and thus, the fibers' distribution and dispersion in the composite material.

Considering all conclusions above, this preliminary research on the production of high quality, high volume fraction composites is deemed to be successful, however, optimization and further research of the process will be necessary to make CFAM an industrially viable production technique.

5 REFERENCES

Bettini, P. et al. 2016. Fused Deposition Technique for Continuous Fiber Reinforced Thermoplastic. *JMEPEG* 26: 843–848.

Brenken, B. et al. 2018. Fused filament fabrication of fiber-reinforced polymers: A review. *Add. Man.* 21: 1-16.

Compton, B. G. et al. 2014. 3D-Printing of Lightweight Cellular Composites. *Add. Man*. 26, 5930–5935.

Compton, B. G. et al. 2017. Thermal analysis of additive manufacturing of large-scale thermoplastic polymer composites. *Add. Man.* 17: 77-86.

Dickson, A. N. et al. 2017. Fabrication of continuous carbon, glass and Kevlar fibre reinforced polymer composites using additive manufacturing. Add. Man. 16: 146–152.

Eichenhofer, M. et al. 2017. Continuous lattice fabrication of ultra-lightweight composite structures. *Add. Man*. 18: 48-57.

Ferreira, R. T. L. et al. 2017. Experimental characterization and micrography of 3D printed PLA and PLA reinforced with short carbon fibers. *Comp. B.* 124: 88-100.

Fu, S.-Y. et al. 2000. Tensile properties of short-glass-fiber- and short-carbon-fiber-reinforced polypropylene composites. *Comp. A* 31: 1117-1125.

Gardner, J. M. et al. 2016. 3-D printing of multifunctional carbon nanotube yarn reinforced components. *Add. Man.* 12: 38-44.

Goh, G. D. et al. 2018. Characterization of mechanical properties and fracture mode of additively manufactured carbon fiber and glass fiber reinforced thermoplastics. *Mat. Des.* 137: 79-89.

Kishore, V. et al. 2017. Infrared preheating to improve interlayer strength of big area additive manufacturing (BAAM) components. *Add. Man.* 14:7-12.

Liu, S. et al. 2018. A novel free-hanging 3D printing method for continuous carbon fiber reinforced thermoplastic lattice truss core structures. *Mat. Des*. 137: 235-244.

Lukaszewicz, D.H.-J.A. et al. 2012. The engineering aspects of automated prepreg layup : History, present and future. *Comp. B* 43: 997-1009.

Matsuzaki, R. et al. 2016. Three-dimensional printing of continuous-fiber composites by in-nozzle impregnation. *Sci. Rep.* 6:23058

Melenka, G. W. et al. 2016. Evaluation and prediction of the tensile properties of continuous fiber-reinforced 3D printed structures. *Comp. Struc*. 153: 866–875.

Nanya, L. et al. 2016. Rapid prototyping of continuous carbon fiber reinforced polylactic acid composites by 3D printing. *Mat. Proc. Tech*. 238: 218-225

Ning, F. et al. 2016. Additive manufacturing of carbon fiber-reinforced plastic composites using fused deposition modeling: Effects of process parameters on tensile properties. *Jour. Comp. Mat.* 0(0) 1–12.

Nunes, J. P. et al. 2003. Production of Powder-Coated Towpregs and Composites. *Therm. Comp. Mat.* 16 (3): 231-248.

Raney, J. R. et al. 2017. Rotational 3D printing of damage-tolerant composites with programmable mechanics, *PNAS.* 115, 6: 1198-1203.

Spoerk, M. et al. 2018. Additive Manufacturing: Effect of Filler